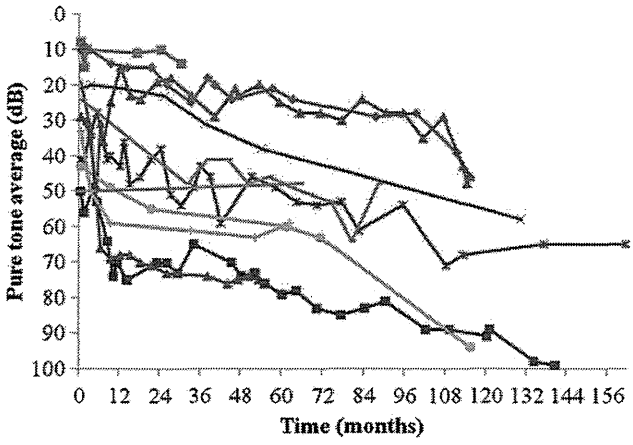

Figure 3. Changes in pure tone average (PTA) of 12 patients after treatment with Hypo-SRT.

control rates in relation to dose fractionation because only 2 cases were progressive, and these patients were given 18 Gy in three fractions and 25 Gy in five fractions, respectively. The results are shown in Table 2. Nine lesions decreased in size, and 15 remained unchanged.

Late Adverse Events

Late adverse events were observed in six patients, and as graded by CTCAE v4.03, these events consisted of Grade 3 hydrocephalus in one patient (4%), Grade 2 facial nerve disorders in two (8%), Grade 1 tinnitus in one (4%) and Grade 2 tinnitus in two (8%) (Table 2). The facial nerve preservation rate was 92%, and the trigeminal nerve preservation rate was 100%. Grade 2 tinnitus occurred in both patients 3 months after Hypo-SRT, and the two cases of Grade 2 facial nerve disorders occurred 7 and 24 months after Hypo-SRT, respectively. The case of Grade 3 hydrocephalus occurred 17 months after Hypo-SRT. The patients with facial nerve disorders recovered rapidly, whereas those with Grade 2 tinnitus required time to recover. The patient with Grade 3 hydrocephalus required hospitalization. The PTV for this patient was 8.4 cm^3, and this patient had to be treated with 25 Gy in five fractions. No trends could be identified for late toxicities in relation to dose fractionation. The prescribed doses for late adverse events in the six lesions were 18 Gy in three fractions for one lesion, 19.5 Gy in three fractions for one lesion, 21 Gy in three fractions for three lesions and 25 Gy in five fractions for one lesion.

The differences in the mean volume of PTV or prescribed dose (NTD 2 Gy, $\alpha/\beta = 3$) between 6 lesions with adverse events and 20 lesions without these events were not significant (2.4 and 4.1 cm^3, respectively, $P = 0.266$; 39.3 and 39.7 Gy, respectively, $P = 0.777$). The mean age at treatment initiation was 58 years for patients with adverse events, compared with 59 years for those without these events ($P = 0.863$). Adverse events occurred for 1 of 6 lesions associated with a background of neurofibromatosis type II and 5 of 20 lesions without that of this disease; the difference was not significant (1/6 and 5/20, $P = 1.000$). No adverse events occurred for the lesions which had undergone prior surgical resection, but occurred for 6 of 20 lesions which had not undergone it; the difference was not significant (0/6 and 6/20, $P = 0.28$).

DISCUSSION

Stereotactic Radiation Therapy for Tumor Control

Historically, SRS or FSRT has often been indicated for vestibular schwannomas. Several studies reported tumor control rates of >90% after the treatment of vestibular schwannomas with SRS (12–16 Gy) or FSRT (50–57.6 Gy) (1–12). Other studies reported similar control rates for Hypo-SRT (17–25 Gy) (13–19). Most of these results as well as ours are listed in Table 3. To evaluate these results accurately, it is important to know the time until progression and the risk factors for progression. Murphy et al. reported that the median time until progression was 32.5 months (1), and Maire et al. reported that tumor progression occurred 12 and 216 months after treatment (2). Delayed tumor progression was observed in some patients (2, 26), and there was one local failure 8 years after Hypo-SRT in this study. Kapoor et al. reported that 10 of 188 tumors with a volume of ≥ 1 cm^3 progressed, whereas only 1 of 197 tumors with a volume of < 1 cm^3 progressed (13). The tumor volume may thus be one of the risk factors for treatment failure. Phi et al. reported that vestibular schwannomas associated with type II neurofibromatosis are considered harder to control than sporadic vestibular schwannomas (27). Although we could not find any significant difference between patients with type II neurofibromatosis and other patients without that disease, special attention may need to be paid to the former, as we experienced one case of progression among patients with that disease.

Adverse Events and Changes in PTA

Facial and trigeminal nerve preservation rates of 73–100% and hearing preservation rates of 0–85% were reported for SRS and FSRT (1–12,23,28,29). For Hypo-SRT, facial and trigeminal preservation rates were 84–100% and hearing preservation rates 61–93% (13–19). Collen et al. reported that the mean tumor diameters were 16.6 mm for the SRS group and 24.6 mm for the FSRT or Hypo-SRT group. Although the local control rates were similar for both the groups, the incidence of facial nerve neuropathy was significantly higher for the groups that underwent SRS or prior surgery, those with larger tumors and those with Koos Grade ≥ 3 (30). The Koos tumor grading classification is as follows: Grade 1 lesions are intracanalicular, Grade 2 lesions have a longitudinal diameter of up to 20 mm, Grade 3 lesions have a longitudinal diameter of up to 30 mm and Grade 4 tumors with a longitudinal diameter of >30 mm can indent and displace the brainstem. It seemed difficult to treat larger tumors with SRS because of the risk of adverse events, and thus, the local control rate

Table 3. Treatment results for vestibular schwannoma after stereotactic radiosurgery (SRS), conventionally fractionated stereotactic radiation therapy (FSRT) or hypofractionated stereotactic radiation therapy (Hypo-SRT)

	n	Dose (Gy)	Fraction	Local control rate (%)	Hearing preservation rate (%)	Facial nerve preservation rate (%)	Trigeminal nerve preservation rate (%)	Follow-up periods (months)
Murphy et al. (1)	117	13	1	91	NA	95	99	38 (Median)
Chopra et al. (4)	216	13	1	98	44	100	95	68 (Median)
Norén (7)	669	NA	1	95	65–70	NA	NA	NA
Kondziolka et al. (9)	162	16	1	98	51	79	73	Between 60 and 120
Iwai et al. (10)	25	12	1	96	64	96	100	89 (Mean)
Szumacher et al. (11)	39	50	25	95	68	95	95	22 (Median)
Maire et al. (2)	45	50.4	28	86	78	100	100	80 (Median)
Fuss et al. (3)	51	57.6	32	98	85	100	96	42 (Mean)
Shirato et al. (5)	65	50	25	92	NA	NA	NA	37 (Mean)
Henzel et al. (12)	39	54	NA	95	NA	NA	NA	36 (Median)
Kapoor et al. (13)	385	25	5	97	NA	98	97	52 (Median)
Meijer et al. (14)	80	25	5	94	61	97	98	33 (Mean)
Sakanaka et al. (15)	12	20	5	92	80	100	100	40 (Median)
Williams (16)	125	25	5	100	NA	100	98	22 (Median)
Chang et al. (17)	61	18	3	98	74	100	97	48 (Mean)
Poen et al. (18)	31	21	3	97	77	97	84	24 (Median)
Ishihara et al. (19)	38	17	3	94	93	100	100	32 (Mean)
This study	25	21	3	95	Six of the 12 patients*	92	100	80 (Median)

n, number of patients; NA, not assessed. *Six of the 12 patients maintained pure tone average (PTA) $\leq$50 dB before and after treatment.

might become lower because of the reduced dose. In fact, the size of the tumors treated with SRS in the report by Collen et al. was smaller than those treated with FSRT or Hypo-SRT (30). Indeed, Hypo-SRT seems to be more effective for treating larger tumors. It is generally considered that the number of adverse events increases with increasing tumor size. In our study, however, adverse events occurred regardless of the tumor volume. The reason may be that the treatment volumes of our cases were too small to reveal significant differences. However, the possibility remains that this study did not have a sufficient number of patients to detect any differences.

Most of the patients in whom PTA was evaluated in our study displayed gradual deterioration during the follow-up. Half of our patients maintained PTAs $\leq$50 dB at the final follow-up. In the natural course of the healthy population, the PTAs were 35 dB in 386 participants aged between 65 and 69 years, and 46.1 dB in 287 participants aged between 75 and 79 years (31). Aging should not be ignored in the deterioration of PTA according to this large population study. In the natural course of untreated vestibular schwannomas (watching policy), hearing preservation rates were 35–45% during follow-up (29,32). Our results appeared to be slightly better than those of the watching group. Among vestibular schwannomas treated with SRS, the hearing preservation rates were 34–64% during follow-up (10,28,33). Our results were intermediate when compared with the SRS groups. Among vestibular schwannomas treated with Hypo-SRT, the hearing preservation rates were 61–93% during follow-up (14,15, 17,19). It was difficult to compare our results with those of previously reported Hypo-SRT groups because our follow-up periods were different. Among vestibular schwannomas treated with FSRT, the hearing preservation rates were 0–78% during follow-up (2,23,29). Our results were intermediate when compared with the FSRT groups.

Our results appeared to be effective in relieving the deterioration of PTA compared with the findings in the watching group. Our results did not appear to be inferior to those of the two groups (SRS and FSRT group), as our results were intermediate between them. An accurate comparison between our results and the Hypo-SRT group was difficult because there was insufficient follow-up PTA information, particularly in the Hypo-SRT group. Our results and those of the other 4 groups (watching, SRS, Hypo-SRT and FSRT group) revealed that it is difficult to avoid decreasing PTA completely during follow-up. The improvement of hearing deterioration in vestibular schwannomas is an issue for future investigation.

POSITIONING OF THIS RESEARCH

This study demonstrated that Hypo-SRT in three to five fractions could be performed safely for vestibular schwannomas although the PTA of the patients deteriorated gradually over time. The finding of tumor progression in a young patient with a background of type II neurofibromatosis indicated that careful attention may have to be paid to the prescribed dose. As there is insufficient information on the results of Hypo-SRT for vestibular schwannomas, especially regarding the use of the CyberKnife, our study provides additional information although the small number of patients is a limitation of this study. In the future, it might be important to consider reducing the total dose to avoid the gradient deterioration of PTA.

In conclusion, Hypo-SRT in three to five fractions for vestibular schwannomas may prevent tumor progression with tolerable toxicity. However, gradient deterioration of PTA was observed.

Acknowledgements

We deeply appreciated the following investigator who contributed to this study: Toshiki Yoshimine M.D. (Department of Neurosurgery, Osaka University Graduate School of Medicine, Suita, Japan). This work was supported in part by the Japan Society for Promotion Science (JSPS) Core-to-Core Program (number 23003).

Funding

This work was supported in part by the Japan Society for Promotion Science (JSPS) Core-to-Core Program (number 23003).

Conflict of interest statement

None declared.

References

1. Murphy ES, Barnett GH, Vogelbaum MA, et al. Long-term outcomes of Gamma Knife radiosurgery in patients with vestibular schwannomas. *J Neurosurg* 2011;114:432–40.
2. Maire JP, Huchet A, Milbeo Y, et al. Twenty years' experience in the treatment of acoustic neuromas with fractionated radiotherapy: a review of 45 cases. *Int J Radiat Oncol Biol Phys* 2006;66:170–8.
3. Fuss M, Debus J, Lohr F, et al. Conventionally fractionated stereotactic radiotherapy (FSRT) for acoustic neuromas. *Int J Radiat Oncol Biol Phys* 2000;48:1381–7.
4. Chopra R, Kondziolka D, Niranjan A, Lunsford LD, Flickinger JC. Long-term follow-up of acoustic schwannoma radiosurgery with marginal tumor doses of 12 to 13 Gy. *Int J Radiat Oncol Biol Phys* 2007;68:845–51.
5. Shirato H, Sakamoto T, Takeichi N, et al. Fractionated stereotactic radiotherapy for vestibular schwannoma (VS): comparison between cystic-type and solid-type VS. *Int J Radiat Oncol Biol Phys* 2000;48:1395–401.
6. Rutten I, Baumert BG, Seidel L, et al. Long-term follow-up reveals low toxicity of radiosurgery for vestibular schwannoma. *Radiother Oncol* 2007;82:83–9.
7. Norén G. Long-term complications following gamma knife radiosurgery of vestibular schwannomas. *Stereotact Funct Neurosurg* 1998;70: 65–73.
8. Pollock BE, Lunsford LD, Kondziolka D, et al. Outcome analysis of acoustic neuroma management: a comparison of microsurgery and stereotactic radiosurgery. *Neurosurgery* 1995;36:215–24; discussion 224–9.
9. Kondziolka D, Lunsford LD, McLaughlin MR, Flickinger JC. Long-term outcomes after radiosurgery for acoustic neuromas. *N Engl J Med* 1998;339:1426–33.
10. Iwai Y, Yamanaka K, Kubo T, Aiba T. Gamma knife radiosurgery for intracanalicular acoustic neuromas. *J Clin Neurosci* 2008;15:993–7.
11. Szumacher E, Schwartz ML, Tsao M, et al. Fractionated stereotactic radiotherapy for the treatment of vestibular schwannomas: combined experience of the Toronto-Sunnybrook Regional Cancer Centre and the Princess Margaret Hospital. *Int J Radiat Oncol Biol Phys* 2002;53: 987–91.
12. Henzel M, Hamm K, Sitter H, et al. Comparison of stereotactic radiosurgery and fractionated stereotactic radiotherapy of acoustic neurinomas according to 3-D tumor volume shrinkage and quality of life. *Strahlenther Onkol* 2009;185:567–73.
13. Kapoor S, Batra S, Carson K, et al. Long-term outcomes of vestibular schwannomas treated with fractionated stereotactic radiotherapy: an institutional experience. *Int J Radiat Oncol Biol Phys* 2011;81:647–53.
14. Meijer OW, Vandertop WP, Baayen JC, Slotman BJ. Single-fraction vs. fractionated linac-based stereotactic radiosurgery for vestibular schwannoma: a single-institution study. *Int J Radiat Oncol Biol Phys* 2003;56:1390–6.
15. Sakanaka K, Mizowaki T, Arakawa Y, et al. Hypofractionated stereotactic radiotherapy for acoustic neuromas: safety and effectiveness over 8 years of experience. *Int J Clin Oncol* 2011;16:27–32.
16. Williams JA. Fractionated stereotactic radiotherapy for acoustic neuromas. *Int J Radiat Oncol Biol Phys* 2002;54:500–4.
17. Chang SD, Gibbs IC, Sakamoto GT, Lee E, Oyelese A, Adler JR, Jr. Staged stereotactic irradiation for acoustic neuroma. *Neurosurgery* 2005;56:1254–61; discussion 1261–3.
18. Poen JC, Golby AJ, Forster KM, et al. Fractionated stereotactic radiosurgery and preservation of hearing in patients with vestibular schwannoma: a preliminary report. *Neurosurgery* 1999;45:1299–305; discussion 1305–7.
19. Ishihara H, Saito K, Nishizaki T, et al. CyberKnife radiosurgery for vestibular schwannoma. *Minim Invasive Neurosurg* 2004;47:290–3.
20. Shiomi H, Inoue T, Nakamura S, Inoue T. Quality assurance for an image-guided frameless radiosurgery system using radiochromic film. *Radiat Med* 2000;18:107–13.
21. Zeman EM. Biologic basis of radiation oncology. In: Gunderson LL, Tepper JE, editors. *Clinical radiation oncology*. 2nd edn. Philadelphia: Elsevier 2007;3–46.
22. Nagano O, Higuchi Y, Serizawa T, et al. Transient expansion of vestibular schwannoma following stereotactic radiosurgery. *J Neurosurg* 2008;109:811–6.
23. Aoyama H, Onodera S, Takeichi N, et al. Symptomatic outcomes in relation to tumor expansion after fractionated stereotactic radiation therapy for vestibular schwannomas: single-institutional long-term experience. *Int J Radiat Oncol Biol Phys* 2013;85:329–34.
24. van de Langenberg R, Dohmen AJ, de Bondt BJ, Nelemans PJ, Baumert BG, Stokroos RJ. Volume changes after stereotactic liniac radiotherapy in vestibular schwannoma:control rate and growth patterns. *Int J Radiat Oncol Biol Phys* 2012;84:343–9.
25. National Cancer Institute. Common terminology criteria for adverse events, Version 4.0. http://evs.nci.nih.gov/ftp1/CTCAE/CTCAE_4.03_2010–06–14_QuickReference_5×7.pdf.
26. Demetriades AK, Saunders N, Rose P, et al. Malignant transformation of acoustic neuroma/vestibular schwannoma 10 years after gamma knife stereotactic radiosurgery. *Skull Base* 2010;20:381–7.
27. Phi JH, Kim DG, Chung HT, Lee J, Paek SH, Jung HW. Radiosurgical treatment of vestibular schwannomas in patients with neurofibromatosis type 2: tumor control and hearing preservation. *Cancer* 2009;115:390–8.
28. Carlson ML, Jacob JT, Pollock BE, et al. Long-term hearing outcomes following stereotactic radiosurgery for vestibular schwannoma: patterns

of hearing loss and variables influencing audiometric decline. *J Neurosurg* 2013;118:579–87.
29. Rasmussen R, Claesson M, Stangerup SE, et al. Fractionated stereotactic radiotherapy of vestibular schwannomas accelerates hearing loss. *Int J Radiat Oncol Biol Phys* 2012;83:e607–11.
30. Collen C, Ampe B, Gevaert T, et al. Single fraction versus fractionated linac-based stereotactic radiotherapy for vestibular schwannoma: a single-institution experience. *Int J Radiat Oncol Biol Phys* 2011;81:e503–9.
31. Yagi M, Kawabata I, Sato T, et al. Hearing acuity in the elderly in Japan. *Nihon Jibiinkoka Gakkai Kaiho* 1996;99:869–74. (in Japanese)
32. Pennings RJ, Morris DP, Clarke L, Allen S, Walling S, Bance ML. Natural history of hearing deterioration in intracanalicular vestibular schwannoma. *Neurosurgery* 2011;68:68–77.
33. Hasegawa T, Kida Y, Kato T, Iizuka H, Yamamoto T. Factors associated with hearing preservation after gamma knife surgery for vestibular schwannomas in patients who retain serviceable hearing. *J Neurosurg* 2011;115:1078–86.

International Journal of
Radiation Oncology
biology • physics

www.redjournal.org

Physics Contribution: Clinical Physics

Estimation of Rectal Dose Using Daily Megavoltage Cone-Beam Computed Tomography and Deformable Image Registration

Yuichi Akino, PhD,*,† Yasuo Yoshioka, MD,* Shoichi Fukuda, MD,§ Shintaroh Maruoka, MD,* Yutaka Takahashi, PhD,*,‖ Masashi Yagi, MS,* Hirokazu Mizuno, MS,† Fumiaki Isohashi, MD,‡ and Kazuhiko Ogawa, MD*

**Department of Radiation Oncology, Osaka University Graduate School of Medicine, Suita; †Department of Radiology and ‡Oncology Center, Osaka University Hospital, Suita; §Department of Radiation Oncology, Osaka General Medical Center, Osaka, Japan; and ‖Department of Radiation Oncology, University of Minnesota, Minneapolis, Minnesota*

Received Mar 18, 2013, and in revised form Jun 19, 2013. Accepted for publication Jun 22, 2013

Summary

Estimating the dose actually delivered to organs that largely deform over the course of radiation therapy is difficult. We developed a method that enables accurate deformable image registration using images with poor image quality, such as megavoltage cone-beam computed tomography. In this study, we characterized the effect of interfractional motion and volume variation on the rectal dose in prostate intensity modulated radiation therapy.

Purpose: The actual dose delivered to critical organs will differ from the simulated dose because of interfractional organ motion and deformation. Here, we developed a method to estimate the rectal dose in prostate intensity modulated radiation therapy with consideration to interfractional organ motion using daily megavoltage cone-beam computed tomography (MVCBCT).

Methods and Materials: Under exemption status from our institutional review board, we retrospectively reviewed 231 series of MVCBCT of 8 patients with prostate cancer. On both planning CT (pCT) and MVCBCT images, the rectal contours were delineated and the CT value within the contours was replaced by the mean CT value within the pelvis, with the addition of 100 Hounsfield units. MVCBCT images were rigidly registered to pCT and then nonrigidly registered using B-Spline deformable image registration (DIR) with Velocity AI software. The concordance between the rectal contours on MVCBCT and pCT was evaluated using the Dice similarity coefficient (DSC). The dose distributions normalized for 1 fraction were also deformed and summed to estimate the actual total dose.

Results: The DSC of all treatment fractions of 8 patients was improved from 0.75 ± 0.04 (mean $\pm$SD) to 0.90 ± 0.02 by DIR. Six patients showed a decrease of the generalized equivalent uniform dose (gEUD) from total dose compared with treatment plans. Although the rectal volume of each treatment fraction did not show any correlation with the change in gEUD ($R^2 = 0.18 \pm 0.13$), the displacement of the center of gravity of rectal contours in the anterior-posterior (AP) direction showed an intermediate relationship ($R^2 = 0.61 \pm 0.16$).

Conclusion: We developed a method for evaluation of rectal dose using DIR and MVCBCT images and showed the necessity of DIR for the evaluation of total dose. Displacement of the rectum in the AP direction showed a greater effect on the change in rectal dose compared with the rectal volume.

Reprint requests to: Yuichi Akino, PhD, Department of Radiation Oncology, Osaka University Graduate School of Medicine, 2-2(D10), Yamadaoka, Suita, Osaka 565-0871, Japan. Tel: (+81) 6-6879-3482; E-mail: akino@radonc.med.osaka-u.ac.jp

Supported by a grant from the Japan Society for the Promotion of Science (JSPS) Core-to-Core Program (No. 23003) and The Osaka Cancer Foundation Award.

Conflict of interest: none.

Acknowledgment—The authors thank Chiyoda Technol Corp (Tokyo, Japan) for providing access to Velocity AI software.

Int J Radiation Oncol Biol Phys, Vol. 87, No. 3, pp. 602–608, 2013
0360-3016/$ - see front matter
http://dx.doi.org/10.1016/j.ijrobp.2013.06.2054

Introduction

Pelvic organs exhibit motion, deformation, and size variation during treatment and over the entire course of radiation therapy (1, 2). Although target dose coverage is maintained by setting a proper planning target volume (PTV) margin, the effect of such organ motion on the dose to organs at risk is difficult to estimate. It is possible to estimate the dose distributions of each treatment fraction by delineation of target volume and critical organs on the image-guided radiation therapy (IGRT) images (2, 3). However, the dose–volume data of multiple fractions cannot be simply summed because unequivocal dose distribution (ie, hot and cold spots) are not located at the same position of the organ.

Recently, deformable image registration (DIR) has attracted attention as a method for automatic contouring, adaptive replanning, and dose accumulation (4-6). In our institution, a clinical trial for image-guided intensity modulated radiation therapy (IMRT) to investigate the optimal PTV margin is currently under way. We collected a large number of megavoltage cone-beam computed tomography (MVCBCT) images of patients who had received prostate IMRT. The image quality of MVCBCT is inferior to that of kilovoltage CT images (7, 8), and identification of soft tissue in the abdominal and pelvic regions remains difficult. Additionally, the use of DIR for the prostate and rectum is challenging because of rectal gas and low contrast, although it works better for thoracic region (9, 10).

Here, we developed a method for the accurate registration of MVCBCT to kilovoltage planning CT (pCT) and estimated the rectal dose in prostate IMRT with consideration to interfractional organ motion.

Methods and Materials

Clinical trial, patients, and MVCBCT image acquisition

Under exemption status from our institutional review board, we started a clinical trial in which the MVCBCT images were acquired for every IMRT fraction using MVision MVCBCT system (Siemens Medical Solutions, Concord, CA). For image acquisition, the range in the superior-inferior (SI) direction was adjusted to 10 cm to reduce the dose to healthy tissue. The imaging dose was 15 MU for all image acquisitions. The treatment protocol included weekly offline correction of the isocenter based on MVCBCT images acquired in the past 1 week and reviewed by 2 radiation oncologists. However, the correction was not performed because a large systematic error was not detected.

We retrospectively analyzed the MVCBCT images of 8 patients with intermediate-risk or high-risk prostate cancer who were treated under this trial between March and November 2011. For these 8 patients, the standard deviations (SDs) of systematic error for left-right (LR), anterior-posterior (AP), and SI directions were 1.46 mm, 1.19 mm, and 0.98 mm, respectively. The PTV was generated by adding 5-mm margins to the prostate and part of the seminal vesicles in all directions. The rectum was defined as a solid structure within the external organ contour and delineated in a range of ±1.5 cm from the edge of the PTV in the SI direction. The treatment planning and dose calculation were performed by use of XiO (version 4.50; Elekta, Stockholm, Sweden) with a 2-mm calculation grid size. A 5-field coplanar treatment plan with beam angles of 45°, 105°, 180°, 255°, and 315° was generated using a 10-MV photon beam for each patient. The imaging dose of MVCBCT was integrated to a prescribed dose of 74 Gy in 37 fractions (11). The patients were instructed to defecate and drink water 1 hour before treatment. The patients were positioned on the basis of their skin surface markers, and MVCBCT images were then acquired. Although MVCBCT images were acquired for every treatment fraction for all patients, some fractions were excluded from this study because of machine error, unacceptable artifacts, and unacceptable rectal gas, which were removed before treatment. The number of acquired MVCBCT image sets was 231 series in total, with a median (minimum-maximum) for each patient of 29 (25-34) series. The workflow of the rectal dose accumulation using DIR and MVCBCT is shown in Figure 1.

Improvement of MVCBCT image noise

We developed in-house software using Microsoft Visual C++ to improve the signal-to-noise ratio. For each slice, the pixel values of the raw DICOM images were replaced by the average of 5 slices: the original slice, the superior 2 slices, and the inferior 2 slices. The pixel data of each image were combined with the header of the original DICOM data and then exported.

We evaluated the image quality with and without averaging technique using a Siemens image-quality phantom, which is a 20-cm diameter cylindrical solid water. At the uniform solid water section, the noise was evaluated by calculating the SD of the region of interest (ROI) located at the center and peripheral 4 positions. The contrast-to-noise ratio (CNR) was also evaluated at the sections that contained rods with various densities. CNR was calculated by the following formula:

$$\mathrm{CNR}=\frac{|\mu_{rod}-\mu_{BG}|}{\sqrt{\sigma_{rod}^2+\sigma_{BG}^2}}$$

where μ and σ represent the mean and SD of CT values inside the ROI located inside the rod or outside (background: BG), respectively.

Contouring on MVCBCT images

The MVCBCT images were imported into the Velocity AI software (version 2.6; Velocity Medical Solutions, Atlanta, GA), and the rectal and bladder contours were delineated. The MVCBCT images and DICOM RT-Struct file exported from Velocity software were imported to in-house software, and the pixels within the rectum were then replaced by the average CT value of the soft tissue within the pelvis on MVCBCT images, with the addition of 100 Hounsfield units. This value is sufficient to enable recognition of the rectum in low-contrast MVCBCT images. The pCT images were processed in the same manner. Figure 2A-B shows an example of the registration of MVCBCT and pCT.

Deformable image registration

The pCT images, MVCBCT images, and DICOM RT-Struct files were again imported into the Velocity software. Using the pCT images as reference, the MVCBCT images of each fraction were rigidly registered. The origin of the MVCBCT images is the first

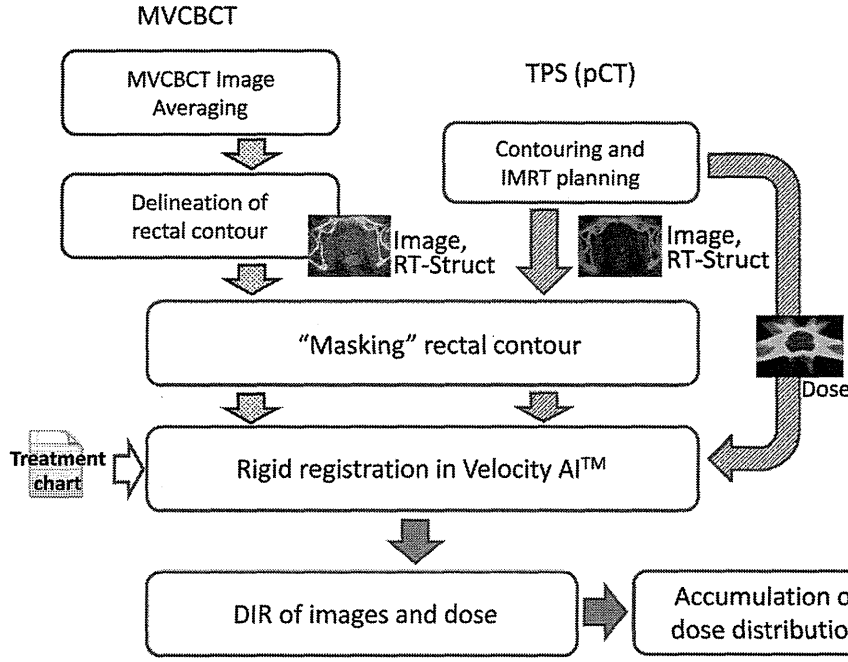

Fig. 1. The workflow of the rectal dose accumulation using deformable image registration (DIR) and megavoltage cone-beam computed tomography (MVCBCT). IMRT = intensity modulated radiation therapy; pCT = planning computed tomography; TPS = treatment planning system.

isocenter coordinate in the patient positions based on skin surface marker. The actual isocenter on MVCBCT can be identified with the image origin and translation distance data of IGRT registered in the treatment record of each patient. In the current study, we defined the rectal volume in the range ±1.5 cm from the edge of the PTV. When applying deformation, the top and bottom slices of the rectum should not be deformed in the SI direction. To limit the deformation of the top and bottom slices of the rectal volume mainly in the transverse directions, the same range in SI direction was used for the rectangular ROI settings for the DIR.

Velocity AI software was used for nonrigid registration (Fig. 2 A-C). Velocity AI uses a calculation algorithm based on modified basis spline (B-Spline) combined with the Mattes formulation of the mutual information metric (12-15). In this algorithm, the deformation vector field, which maps voxels in the target image to those in the reference image, is interpolated between grid points using a cubic spline curve. Lawson et al (14) previously reported that the average error of the DIR on noise-free images using this algorithm was less than 1 mm, with a maximum of 2 mm. The dose of the treatment plan was normalized for 1 fraction (2 Gy for 95% volume of PTV), and the DICOM RT-Dose file was exported from XiO. Copies of the dose file were created for the number of MVCBCT image series and imported into the Velocity software. The dose distributions were registered to the MVCBCT of each fraction, and the dose distributions were then also deformed using the pCT-MVCBCT deformation data (Fig. 2 D-E).

Evaluation of rectal and bladder doses

To evaluate the concordance between the contours of the rectum for MVCBCT with and without deformation and that of the pCT, the Dice similarity coefficient (DSC) (16) was calculated by the following formula:

$$\mathrm{DSC} = \frac{2(N_{pCT} \cap N_{MV})}{N_{pCT} + N_{MV}}$$

where N_{pCT} and N_{MV} represent the number of voxels within the rectal contours identified on the pCT and MVCBCT, respectively. The DSC values are close to unity for 2 concordant contours. Resolution for the DSC calculation was half the pixel size of a pCT image in the transverse plane (0.49 mm) and the same for slice thickness in the SI direction (2.5 mm).

For the assessment of rectal dose, the generalized equivalent uniform dose (gEUD) proposed by Niemierko (17) was calculated as follows:

$$\mathrm{gEUD} = \left(\sum_i \frac{V_i}{V} D_i^{1/n} \right)^n$$

where n is a parameter that describes the volumetric dependence of the dose–response relationship for each organ. When $n = 1$, the gEUD value is equal to the mean dose, and a lower n value indicates stronger high-dose sensitivity. The gEUD represents the homogeneous dose distribution that results in the same probability of complications as that of an inhomogeneous dose distribution. The values of n were 0.12, as Burman et al (18) previously reported. The dose delivered to the 2% volume of the rectum ($D_{2\%}$) was also evaluated as a parameter of the maximum dose. The accumulated DVH was scaled up with consideration to the prescribed treatment fractions and the number of treatments with MVCBCT image acquisition to compare the data with treatment plans. The volumes receiving a certain dose (Vx) were analyzed to evaluate bladder dose with stretching contours.

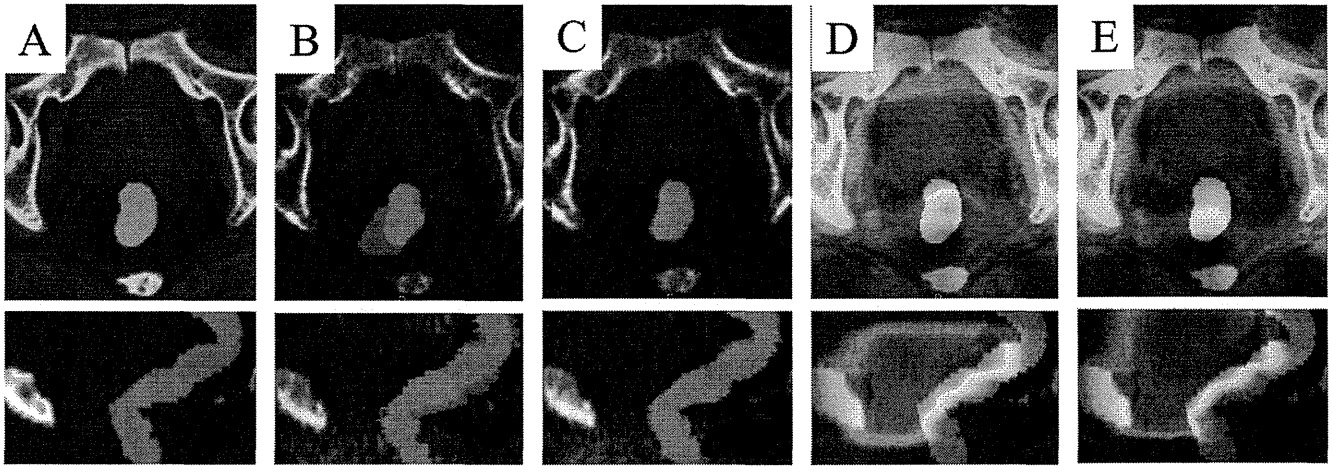

Fig. 2. Registration of planning computed tomographic (A) and megavoltage cone-beam computed tomographic images using rigid (B) and deforming (C) methods. (C, D) Dose distribution of the treatment plan is overlapped on the pCT image. Dose distributions were registered using rigid (D) and deforming (E) methods.

Statistical analysis

The differences between DSC values with and without DIR were compared with the 2-tailed paired *t* test by use of JMP Software (SAS Institute, Cary, NC). The Wilcoxon signed-rank test was used to compare the dosimetric parameters between plans and accumulated doses. Statistical significance was set at $P<.05$.

Results

The effects of the averaging technique on the improvement of image quality are shown in Figure 3A-C. The noise was reduced on average 37.9% by averaging technique. The CNR was also improved by slice averaging (Fig. 3C).

Figure 4A represents the variation in the rectal volume of each treatment fraction from the volume of pCT. For patients 1, 2, 5, and 7, the rectal volume on pCT was almost at the middle of all treatment fractions. By contrast, other cases showed systematically larger (patients 3 and 6) or smaller (patients 4 and 8) rectal volumes on MVCBCT compared with the volumes on pCT ($P<.01$). Figure 4B-C shows the box-whisker plot of DSC between the rectal contour of pCT and each MVCBCT before and after deformation, respectively. For rigid registrations (Fig. 4B), the average DSC of all treatment fractions of 8 patients was 0.75±0.04 (SD). After deformation, this value was significantly improved to 0.90±0.02 ($P<.0001$).

The comparison between the planned and accumulated doses to the rectum and bladder is shown in Table 1. The rectal gEUD and $D_{2\%}$ of the accumulated dose showed statistically significant decreases compared with those of the planned doses ($P=.039$ and $P=.016$, respectively). The bladder volumes receiving ≥70 Gy ($V_{70\ Gy}$) and ≥60 Gy ($V_{60\ Gy}$) are also given in Table 1. Some cases showed increases of $V_{70\ Gy}$ and $V_{60\ Gy}$, although there was no significant difference between planned and accumulated doses.

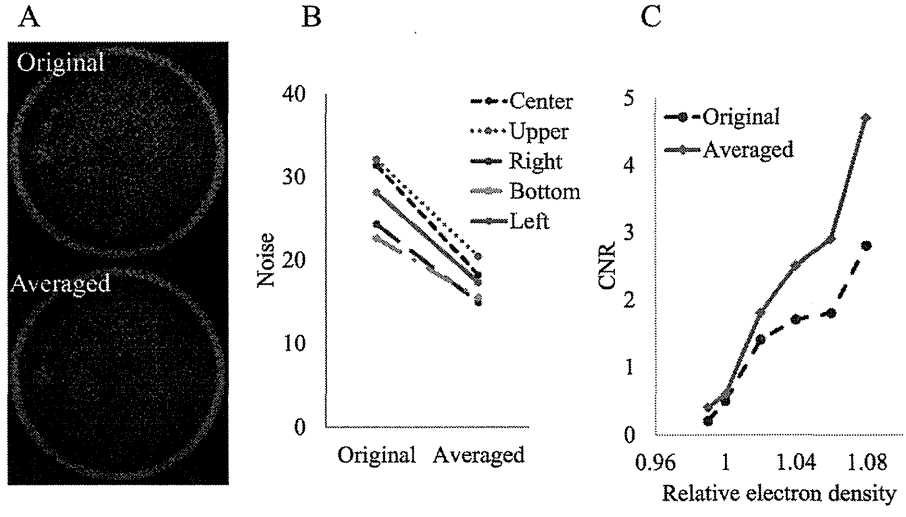

Fig. 3. (A) Megavoltage cone-beam computed tomographic (MVCBCT) images of Siemens image quality phantom without (original) and with (averaged) averaging technique. (B) Noise measurement at 5 points on the phantom images. (C) Contrast-to-noise ratio (CNR) of MVCBCT images. X-axis represents the electron density of the rods relative to water.

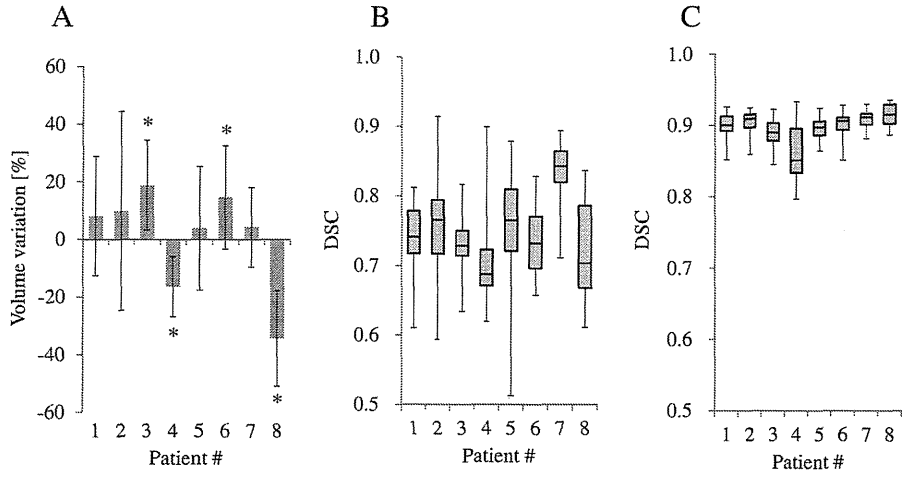

Fig. 4. (A) Variation in rectal volume in individual patients. Columns represent the difference between the volume on planning computed tomography and the averaged volume. Bars show the ±SD. $^{*}P<.01$ (*t* test, comparison between volumes on megavoltage cone-beam computed tomography and planning computed tomography). Dice similarity coefficient (DSC) of rectal volume before (B) and after (C) deformable image registration is summarized as standard whisker-box plots. Boxes symbolize the 50% range of treatment fractions (median ±25%), and whiskers represent the maximum and minimum range.

In Figure 5A, the difference in gEUD between each fraction and the treatment plans are plotted with the rectal volume of the each fraction relative to the volume on pCT. No correlation was found ($R^2=0.18\pm0.13$). In Figure 5B, the gEUD difference in each fraction was plotted with displacement of the rectal center of gravity in the AP direction from the rectal center of gravity at treatment planning. Figure 5C shows a linear approximation of the correlation between AP displacement of the rectum and gEUD for each patient. An intermediate correlation was found ($R^2=0.61\pm0.16$).

Discussion

Many studies have demonstrated an association between late rectal toxicity and high dose (>60 Gy), although a few have reported that rectal bleeding also correlates with the volume exposed to intermediate doses (40-60 Gy) (19, 20). In actual treatment, the high-dose region will be displaced in every fraction, resulting in a blurred dose distribution. We demonstrated that the effects of interfractional motion in the AP direction showed an intermediate correlation with the rectal gEUD (Fig. 5B-C). The rectal gEUD is highly sensitive to high doses because of the small-value *n*; the radiobiologic dose–volume effect parameter. This result indicates that the management of rectal conditions is important to reduce rectal complications. Because some organs show a large size variation in the course of radiation therapy, DIR will be essential to evaluate the effects of interfractional motion and deformation properly. Although many reports have described the use of DIR and various IGRT modalities, including kilovoltage cone-beam CT (kV-CBCT), tomotherapy, and in-room CT (21-23), few reports have used MVCBCT images for DIR. This is likely because of the higher imaging dose of MVCBCT compared to other imaging modalities and the poor image quality of MVCBCT. Morrow et al (7) compared interobserver and intraobserver errors in the realignment of various IGRT images, including in-room CT, kV-CBCT, tomotherapy, and MVCBCT and concluded that the quality of MVCBCT was the worst of these modalities. Although

Table 1 Dosimetric comparison between planned and accumulated doses for each patient

	Rectum				Bladder			
	gEUD (Gy)*		$D_{2\%}$ (Gy)†		$V_{70\ Gy}$ (cm^3)		$V_{60\ Gy}$ (cm^3)	
Patient	Plan	Accum	Plan	Accum	Plan	Accum	Plan	Accum
1	63.2	64.1	77.1	76.4	14.3	18.4	23.3	30.7
2	55.3	56.8	73.8	74.3	2.1	1.6	4.9	4.8
3	60.9	56.5	75.9	73.2	21.7	27.5	38.1	45.7
4	59.3	53.8	75.8	71.7	12.8	13.0	16.8	18.3
5	59.7	56.8	75.9	72.8	6.3	7.6	12.6	17.7
6	59.8	55.2	76.1	72.7	27.0	27.7	39.7	43.9
7	58.9	55.7	75.7	72.6	11.8	11.1	19.7	19.8
8	58.2	51.3	74.6	69.0	25.9	24.6	37.8	36.1

Abbreviations: Accum = accumulated; gEUD = generalized equivalent uniform dose.
* $P=.039$.
† $P=.016$.

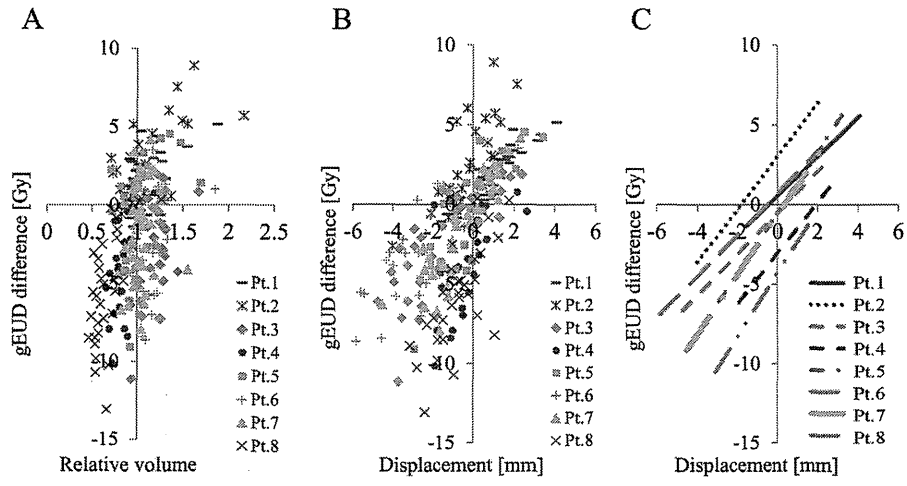

Fig. 5. Differences in generalized equivalent uniform dose (gEUD) between the dose of treatment plans and each treatment fraction as plotted with (A) rectal volume and (B) displacement of the rectal center of gravity in the anterior-posterior direction. (C) Linear approximation of the correlation between gEUD difference and rectal displacement in the anterior-posterior direction for each patient. In Figure B and C, the positive and negative values in x-axis represent shifts in the anterior and posterior directions, respectively.

observers who routinely use MVCBCT will achieve much better results, an improvement in image quality is nevertheless required to ensure the accuracy desired for DIR.

The first problem can be solved by using imaging-dose integration to the prescribed dose. Morin et al (24) and Miften et al (25) showed a method for incorporating the MVCBCT dose to the prescribed dose. The effect of imaging dose integration on the prostate IMRT dose distribution has also been reported (11). These methods enable daily image acquisition with MVCBCT and minimize dose increases to the patient's body.

In the present study, we demonstrated a solution for the second problem. We demonstrated that the DSC was improved from 0.75 to 0.90 by DIR. Kirby et al (10) compared 11 DIR algorithms using kilovoltage CT images of phantom and reported that the DSC of the rectum was on average 0.85 after DIR, whereas the DSC without DIR was 0.68. With our technique, the accuracy of DIR with MVCBCT was improved to the similar level of DIR with kilovoltage CT. Yang et al (22) previously showed a similar method for precise DIR. They scaled the CT value up or down in the bladder, prostate, and rectum on tomotherapy MVCT images and showed that this improved the accuracy of registration, although they did not evaluate the accumulated dose. We focused on the rectal dose in this study. As shown in Figure 2C,E, the DIR outside masked contour was not correct at all. This means that the masking technique is essential for deforming MVCBCT images. Such inappropriate deformations will not affect the DVH assessment of masked contours.

Wen et al (26) investigated the accumulated dose in prostate IMRT using daily kV-CBCT and DIR. They reported that the rectal gEUD was increased for all 5 cases. However, they did not investigate the correlation between the rectal dose and condition of the rectum, including its volume and position. This study revealed that an increase in rectal volume by rectal gas or feces is not always accompanied by an increase in rectal dose (Figure 5A). If the rectum is shifted in the posterior direction, it will be far from the high-dose region, resulting in a decrease in rectal dose. Peng et al (2) previously investigated the interfractional organ motion of the prostate, bladder, and rectum using daily in-room CT image acquisition and found that approximately 30% of treatment fractions showed large organ deformation and rotations, which could not be corrected by translational shifts. For target coverage, this problem should be resolved by repositioning, PTV margin, and/or on-line adaptation of treatment. Godley et al (23) reported the cumulative rectal and bladder dose using daily in-room CT images and DIR and showed that the effect of interfractional organ motion on rectal and bladder dose was larger than that on target coverage. We found that position in the AP direction was critical for dose variation, although rectal volume was not correlated. When patient realignment is considered, subsequent movement caused by rectal filling should then be considered.

The uncertainties of DIR include accuracy of the deformation vector field between 2 image sets and of the dose warping. Several studies have investigated the accuracy of the DIR using phantom studies (10, 14). We consider that the masking with manual contouring partly reduced the uncertainty in the deformation of images with poor image qualities, although the uncertainty resulting from interobserver or intraobserver error should be considered (7). Some studies have also investigated the accuracy of dose warping (4, 27, 28). Yeo et al (27) pointed out the uncertainty in the deformation accuracy in the region with low contrast. In the current study, the uncertainty of the registration at the middle of the contours may be larger than in the peripheral region because of the uniform density. Further investigations are needed to overcome such problems. The use of this method in routine clinical treatment will be hampered by the time-consuming need to manually delineate the rectum for every treatment fraction. However, our finding may be helpful when realignment strategies using pelvic IGRT are considered. The limitations of this method include the fact that the dose distribution is not recalculated. For prostate cancer patients, the variation of the path length in each treatment may be negligible because of stable patient size. For patients with changes in body size (ie, those with head-and-neck cancer), recalculation will be necessary before DIR.

Conclusion

A method was developed to estimate the rectal dose with consideration of interfractional organ motion using daily MVCBCT and DIR. By use of this technique, rectal volume on MVCBCT images of each treatment fraction was properly

deformed to the reference volume on pCT. Rectal dose changes are more sensitive to displacement in the AP direction than to rectal volume.

References

1. Kerkhof EM, van der Put RW, Raaymakers BW, et al. Variation in target and rectum dose due to prostate deformation: An assessment by repeated MR imaging and treatment planning. *Phys Med Biol* 2008;53: 5623-5634.
2. Peng C, Ahunbay E, Chen G, et al. Characterizing interfraction variations and their dosimetric effects in prostate cancer radiotherapy. *Int J Radiat Oncol Biol Phys* 2011;79:909-914.
3. Song WY, Wong E, Bauman GS, et al. Dosimetric evaluation of daily rigid and nonrigid geometric correction strategies during on-line image-guided radiation therapy (IGRT) of prostate cancer. *Med Phys* 2007;34:352-365.
4. Janssens G, de Xivry JO, Fekkes S, et al. Evaluation of nonrigid registration models for interfraction dose accumulation in radiotherapy. *Med Phys* 2009;36:4268-4276.
5. Godley A, Ahunbay E, Peng C, et al. Automated registration of large deformations for adaptive radiation therapy of prostate cancer. *Med Phys* 2009;36:1433-1441.
6. Ahunbay EE, Peng C, Godley A, et al. An on-line replanning method for head and neck adaptive radiotherapy. *Med Phys* 2009;36:4776-4790.
7. Morrow NV, Lawton CA, Qi XS, et al. Impact of computed tomography image quality on image-guided radiation therapy based on soft tissue registration. *Int J Radiat Oncol Biol Phys* 2012;82:e733-e738.
8. Stutzel J, Oelfke U, Nill S. A quantitative image quality comparison of four different image guided radiotherapy devices. *Radiother Oncol* 2008;86:20-24.
9. Brock KK. Results of a multi-institution deformable registration accuracy study (MIDRAS). *Int J Radiat Oncol Biol Phys* 2010;76:583-596.
10. Kirby N, Chuang C, Ueda U, et al. The need for application-based adaptation of deformable image registration. *Med Phys* 2013;40:011702.
11. Akino Y, Koizumi M, Sumida I, et al. Megavoltage cone beam computed tomography dose and the necessity of reoptimization for imaging dose-integrated intensity-modulated radiotherapy for prostate cancer. *Int J Radiat Oncol Biol Phys* 2012;82:1715-1722.
12. Rueckert D, Sonoda LI, Hayes C, et al. Nonrigid registration using free-form deformations: Application to breast MR images. *IEEE Trans Med Imaging* 1999;18:712-721.
13. Shackleford JA, Kandasamy N, Sharp GC. On developing B-spline registration algorithms for multi-core processors. *Phys Med Biol* 2010; 55:6329-6351.
14. Lawson JD, Schreibmann E, Jani AB, et al. Quantitative evaluation of a cone-beam computed tomography-planning computed tomography deformable image registration method for adaptive radiation therapy. *J Appl Clin Med Phys* 2007;8:2432.
15. Mattes D, Haynor DR, Vesselle H, et al. PET-CT image registration in the chest using free-form deformations. *IEEE Trans Med Imaging* 2003;22:120-128.
16. Zou KH, Warfield SK, Bharatha A, et al. Statistical validation of image segmentation quality based on a spatial overlap index. *Acad Radiol* 2004;11:178-189.
17. Niemierko A. A generalized concept of equivalent uniform dose (EUD). *Med Phys* 1999;26:1100 [Abstract].
18. Burman C, Kutcher GJ, Emami B, et al. Fitting of normal tissue tolerance data to an analytic function. *Int J Radiat Oncol Biol Phys* 1991;21:123-135.
19. Michalski JM, Gay H, Jackson A, et al. Radiation dose-volume effects in radiation-induced rectal injury. *Int J Radiat Oncol Biol Phys* 2010; 76:S123-S129.
20. Jackson A, Skwarchuk MW, Zelefsky MJ, et al. Late rectal bleeding after conformal radiotherapy of prostate cancer. II. Volume effects and dose-volume histograms. *Int J Radiat Oncol Biol Phys* 2001;49: 685-698.
21. Jones BL, Gan G, Diot Q, et al. Dosimetric and deformation effects of image-guided interventions during stereotactic body radiation therapy of the prostate using an endorectal balloon. *Med Phys* 2012; 39:3080-3088.
22. Yang D, Chaudhari SR, Goddu SM, et al. Deformable registration of abdominal kilovoltage treatment planning CT and tomotherapy daily megavoltage CT for treatment adaptation. *Med Phys* 2009;36:329-338.
23. Godley A, Ahunbay E, Peng C, et al. Accumulating daily-varied dose distributions of prostate radiation therapy with soft-tissue-based kV CT guidance. *J Appl Clin Med Phys* 2012;13:3859.
24. Morin O, Gillis A, Descovich M, et al. Patient dose considerations for routine megavoltage cone-beam CT imaging. *Med Phys* 2007;34: 1819-1827.
25. Miften M, Gayou O, Reitz B, et al. IMRT planning and delivery incorporating daily dose from mega-voltage cone-beam computed tomography imaging. *Med Phys* 2007;34:3760-3767.
26. Wen N, Glide-Hurst C, Nurushev T, et al. Evaluation of the deformation and corresponding dosimetric implications in prostate cancer treatment. *Phys Med Biol* 2012;57:5361-5379.
27. Yeo UJ, Taylor ML, Supple JR, et al. Is it sensible to "deform" dose? 3D experimental validation of dose-warping. *Med Phys* 2012; 39:5065-5072.
28. Bender ET, Hardcastle N, Tome WA. On the dosimetric effect and reduction of inverse consistency and transitivity errors in deformable image registration for dose accumulation. *Med Phys* 2012;39:272-280.

Journal of Radiation Research, 2013, 54, 781–788
doi: 10.1093/jrr/rrt027 Advance Access Publication 29 March 2013

Review

The emerging role of high-dose-rate (HDR) brachytherapy as monotherapy for prostate cancer

Yasuo YOSHIOKA[1,*], Ken YOSHIDA[2], Hideya YAMAZAKI[3], Norio NONOMURA[4] and Kazuhiko OGAWA[1]

[1]Department of Radiation Oncology, Osaka University Graduate School of Medicine, 2-2 Yamadaoka, Suita, Osaka 565-0871, Japan
[2]Department of Radiology, Osaka Medical College, 2-7 Daigaku-machi, Takatsuki, Osaka 569-8686, Japan
[3]Department of Radiology, Kyoto Prefectural University of Medicine, 465 Kajiicho Kawaramachi Hirokoji, Kamigyo-ku, Kyoto 602-8566, Japan
[4]Department of Urology, Osaka University Graduate School of Medicine, 2-2 Yamadaoka, Suita, Osaka 565-0871, Japan
*Corresponding author. Tel: +81-6-6879-3482; Fax: +81-6-6879-3489; Email: yoshioka@radonc.med.osaka-u.ac.jp

(Received 22 January 2013; revised 26 February 2013; accepted 2 March 2013)

High-dose-rate (HDR) brachytherapy as monotherapy is a comparatively new brachytherapy procedure for prostate cancer. In addition to the intrinsic advantages of brachytherapy, including radiation dose concentration to the tumor and rapid dose fall-off at the surrounding normal tissue, HDR brachytherapy can yield a more homogeneous and conformal dose distribution through image-based decisions for source dwell positions and by optimization of individual source dwell times. Indication can be extended even to T3a/b or a part of T4 tumors because the applicators can be positioned at the extracapsular lesion, into the seminal vesicles, and/or into the bladder, without any risk of source migration or dropping out. Unlike external beam radiotherapy, with HDR brachytherapy inter-/intra-fraction organ motion is not problematic. However, HDR monotherapy requires patients to stay in bed for 1–4 days during hospitalization, even though the actual overall treatment time is short. Recent findings that the α/β value for prostate cancer is less than that for the surrounding late-responding normal tissue has made hypofractionation attractive, and HDR monotherapy can maximize this advantage of hypofractionation. Research on HDR monotherapy is accelerating, with a growing number of publications reporting excellent preliminary clinical results due to the high 'biologically effective dose (BED)' of >200 Gy. Moreover, the findings obtained for HDR monotherapy as an early model of extreme hypofractionation tend to be applied to other radiotherapy techniques such as stereotactic radiotherapy. All these developments point to the emerging role of HDR brachytherapy as monotherapy for prostate cancer.

Keywords: prostate cancer; high-dose-rate (HDR); brachytherapy; monotherapy; hypofractionation

INTRODUCTION

Multiple treatment options are available for clinically localized prostate cancer, including radical prostatectomy, external beam radiotherapy (EBRT), brachytherapy, and a combination of EBRT and brachytherapy. Brachytherapy in the form of a permanent low-dose-rate (LDR) seed implant, or as high-dose-rate (HDR) afterloading, can deliver a highly localized radiation dose to the tumor. While LDR brachytherapy has been examined and assessed the most and become a standard treatment option, HDR brachytherapy is recently gaining momentum as an alternative. Several features of HDR brachytherapy, including uniformly accurate, precise, and reproducible dosimetry resulting from its advanced optimization capabilities, radiobiological and radioprotective advantages, and reduced costs, have made HDR attractive for the treatment of prostate cancer. These advantages avoid the dosimetric uncertainties of LDR related to postimplant volume changes due to needle trauma and subsequent edema during the several months of overall treatment time. HDR significantly improves the radiation dose distribution because it can

modulate and accurately control both the spatial source position and dwell time during treatment.

Historically, HDR brachytherapy was introduced to boost EBRT [1, 2]. Accumulation of clinical results for EBRT and HDR brachytherapy combination therapy culminated in recommendations by the Groupe Européen de Curiethérapie (GEC)/European Society for Radiotherapy and Oncology (ESTRO)-European Association of Urology (EAU) [3], and consensus guidelines by the American Brachytherapy Society (ABS) [4]. However, this combination typically adds 4–5 weeks to the time needed for completion of EBRT, in addition to hospitalization for HDR brachytherapy. HDR brachytherapy as monotherapy, on the other hand, would definitely be the most efficient method of achieving a high degree of conformity and dose escalation. The aim of this paper is to review the literature to date for HDR brachytherapy as monotherapy and to discuss its function and future direction.

HISTORY AND INDICATION

Tables 1 and 2 list as many data on dose fractionation and its clinical results as we could collect from the literature on HDR brachytherapy as monotherapy for prostate cancer [5–22]. Our search resulted in a total of approximately 20 articles from only 11 institutions worldwide. The number of dose-fractionation schedules used was larger than the number of institutions because some institutions adopted several dose-fractionation schedules, mostly involving dose escalation. Since very few institutions were using HDR monotherapy in the 1990s, relevant articles published in the 2000s were also very few. In the 2000s, however, a growing number of institutions started to use HDR monotherapy, so that the number of germane papers published in the 2010s has also been increasing.

In the first article on HDR monotherapy from Osaka University, Japan, published in 2000, the authors reported they had initiated HDR monotherapy in 1995, with indications for low- to high-risk prostate cancer [5]. Two subsequent articles, however, one from the William Beaumont Hospital in the USA (2001) [6] and the other from Klinikum Offenbach in Germany (2004) [7], reported that indications were limited to low- or low-to-intermediate-risk patients. As a result, some investigators maintained that HDR monotherapy was suitable only for low or low-to-intermediate risk, and a combination of EBRT and HDR brachytherapy for intermediate- to high-risk patients, thus emulating the scheme for LDR brachytherapy. On the other hand, a subsequent report from Mount Vernon Cancer Centre in the UK published in 2008 [8] mentioned the inclusion of high-risk patients, and in their second report (2012) [9], the authors clearly stated that they had indicated HDR monotherapy mainly for intermediate- and high-risk groups. Similarly, radiation oncologists at Osaka University have been limiting their indications to intermediate- and high-risk groups since 2005 (and LDR brachytherapy to low-risk patients) (Y. Yoshioka *et al.*, submitted for publication). According to the second report from Klinikum Offenbach published in 2013 [10], indications had been extended to high-risk patients. Of their 226 patients, who were treated with their latest protocol using 34.5 Gy in three fractions with three implants, 42% were low-, 32% intermediate-, and 25% high-risk patients. A report from the GammaWest Cancer Services in Salt Lake City, UT published in 2012 listed the clinical results of HDR monotherapy for 284 intermediate-risk patients [11]. All these recent studies clearly indicate that limiting indications for HDR monotherapy to low-risk patients is no longer viable, and such indications now tend to be extended to high-risk patients.

However, one should be aware of the possibility of micrometastases to pelvic lymph nodes, especially in high-risk patients. The Radiation Therapy Oncology Group (RTOG) 9413 study showed superiority of whole-pelvic RT to prostate-only RT on progression-free survival [23, 24]. This may imply that whole-pelvic RT plus HDR brachytherapy boost, or simultaneous integrated boost intensity-modulated RT (SIB-IMRT), e.g., is more suitable for such high-risk patients. In contrast, some authors have denied the benefit of pelvic RT in high-risk patients of positive pelvic lymph nodes treated with high-dose radiation [25]. On the other hand, local dose escalation has been questioned many times concerning whether it is associated with decreasing disease-specific mortality [26]. Overall, the benefit of whole-pelvic RT or local dose escalation to overall survival is still in debate [27, 28], and investigators of HDR monotherapy, an ideal tool for local dose escalation which avoids whole-pelvic RT, are recommended to take this issue into consideration when they apply such a treatment to intermediate- to high-risk patients.

EQUIPMENT AND RADIATION PHYSICS

(i) Because the dose-rate of the radioactive source is high, a remote afterloading system (RALS) or an HDR unit, which is now commonly used for intracavitary brachytherapy for uterine cervix cancer, is essential. A typical HDR unit involves one ^{192}Ir stepping source, 4.5 mm in length and 0.9 mm in diameter, which has a radioactivity of 370 GBq at the time of certification. ^{192}Ir has an average energy of 370 keV and a half-life of 73.8 days.

(ii) Under lumbar or epidural anesthesia, plastic or metallic needle applicators are inserted via the perineum into the prostate gland with the aid of real-time transrectal ultrasound (TRUS) guidance. TRUS is usually equipped with a template that is used to determine placement of the needles. The

Table 1. Dose fractionation and BED of prostate HDR brachytherapy as monotherapy

Author [ref.]	Institution	Country	Start (year)	Publication (year)	HDR physical dose			BED (Gy)		EQD_{2Gy} (Gy)	
					Dose/ fraction	No. of fractions	Total dose	α/β = 1.5 Gy	α/β = 3.0 Gy	α/β = 1.5 Gy	α/β = 3.0 Gy
Yoshioka [5, submitted for publication, 19–21]	Osaka University	Japan	1995	2000	6 Gy	8	48 Gy	240	144	103	86
			1996	2011	6 Gy	9	54 Gy	270	162	116	97
			2005	in submission	6.5 Gy	7	45.5 Gy	243	144	104	86
Demanes [12]	California Endocurietherapy	USA	1996	2011	7 Gy	6 (2 implants)	42 Gy	238	140	102	84
Martinez [6, 18, 22]	William Beaumont Hospital	USA	1999	2010	9.5 Gy	4	38 Gy	279	158	119	95
			2005	2012	12 Gy	2	24 Gy	216	120	93	72
					13.5 Gy	2	27 Gy	270	149	116	89
Rogers [11]	Salt Lake City	USA	2001	2012	6.5 Gy	6 (2 implants)	39 Gy	208	124	89	74
Zamboglou [7, 10]	Klinikum Offenbach	Germany	2002	2004	9.5 Gy	4	38 Gy	279	158	119	95
				2013	9.5 Gy	4 (2 implants)	38 Gy	279	158	119	95
					11.5 Gy	3 (3 implants)	34.5 Gy	299	167	128	100
Hoskin [8, 9]	Mount Vernon Hospital	UK	2003	2008	8.5 Gy	4	34 Gy	227	130	97	78
					9 Gy	4	36 Gy	252	144	108	86
					10.5 Gy	3	31.5 Gy	252	142	108	85
				2012	13 Gy	2	26 Gy	251	139	108	83
Ghadjar [13]	University of Bern	Switzerland	2003	2009	9.5 Gy	4	38 Gy	279	158	119	95
Barkati [14]	Melbourne	Australia	2003	2012	10 Gy	3	30 Gy	230	130	99	78
					10.5 Gy	3	31.5 Gy	252	142	108	85
					11 Gy	3	33 Gy	275	154	118	92
					11.5 Gy	3	34.5 Gy	299	167	128	100
Yoshida [15]	Osaka National Hospital	Japan	2004	2010	7 Gy	7	49 Gy	278	163	119	98
					6 Gy	9	54 Gy	270	162	116	97
					9.5 Gy	4	38 Gy	279	158	119	95
Komiya [16]	University of Toyama	Japan	2007	2013	6.5 Gy	7	45.5 Gy	243	144	104	86
Prada [17]	Asturias	Spain	2008	2012	19 Gy	1	19 Gy	260	139	111	84

BED = biologically effective dose, HDR = high-dose-rate, EQD_{2Gy} = biologically equivalent dose in 2-Gy fractions.

template has many holes for the needles to pass through, and their positions are superimposed on the TRUS monitor in advance. The tips of these needles tip are closed, unlike the ones used for LDR permanent seed implants.

(iii) Treatment planning is based on the computed tomography (CT) images obtained after needle insertion, or on the TRUS images obtained at the time of needle insertion. The dwell positions of the stepping source are determined in terms of real anatomy, that is, of the actual condition with the needles inserted. The dwell time for each dwell position is then calculated with an optimization algorithm.

(iv) Medical staff are never exposed to radiation, and patients can stay in a regular ward since there is no need for a shielded room. Patients only need to go to a RALS room for irradiation, which takes approximately 10 minutes per fraction.

(v) Radiation dose from the source obeys the inverse square law. This means that the dose to the region outside the planning target volume (PTV) decreases rapidly, thus sparing the surrounding normal tissue. This process is visible as a rapid dose fall-off on a dose distribution plot.

(vi) Unlike for EBRT, inter-/intra-fraction organ motion is not a problem with HDR brachytherapy. In the case of EBRT, several factors including daily set-up errors, retention of feces, gas, or urine, respiratory motion, or peristaltic motion result in discrepancies between the coordinates of the tumor and the radiation beam. With brachytherapy, on the other hand, these two coordinates are always concordant because the tumor and the radioactive sources move in unison, so that PTV is normally identical to the clinical target volume (CTV). However, needle displacement is problematic with HDR brachytherapy (see (viii) below). The overall treatment time for HDR monotherapy typically ranges from 1–4 days, which is significantly shorter than for EBRT.

(vii) Unlike for LDR brachytherapy, HDR brachytherapy needles can be placed at the extracapsular lesion, and even into the seminal vesicles and/or into the bladder pouch, if necessary. The cable-connected stepping source simply moves back and forth within the closed space without any risk of source migration or dropping out. Therefore, the indication for HDR monotherapy can potentially be extended to even T3a/b or some T4 tumors. The above-mentioned dwell time optimization makes a significant urethral dose reduction possible for HDR compared to that for LDR.

(viii) One of the drawbacks of HDR brachytherapy is the problem of needle applicator displacement during treatment [6, 15, 29–34]. To overcome this problem, some radiation oncologists use daily CT scans to adjust needle positions or source dwell positions or use roentgenography to readjust the relative locations of the implanted fiducial markers and the needles. Another drawback of HDR is the requirement of hospitalization and patients having to stay in bed during the treatment period. As for the latter problem, treatment periods tend to become shorter with an increase in the fraction size (see the next section). Some practitioners have even adopted a multiple-implant schedule with a single fraction irradiation for each implant, which avoids the disadvantages of both needle displacement and hospitalization [10].

RADIATION BIOLOGY AND DOSE FRACTIONATION

The α/β value of prostate cancer is considered to be significantly lower than that of other cancers such as of the lung, or of the head and neck. In 1999, Brenner and Hall published a groundbreaking paper on this issue, in which they asserted that the α/β value of prostate cancer was 1.5 Gy [35]. This has been followed by a significant number of publications reporting α/β values mostly in the range of 1.2 – 3.1 Gy [36–39]. For the rest of this paper we will use $\alpha/\beta = 1.5$ Gy because we consider it to be closest to the standard value. On the other hand, the α/β value for late-responding normal tissue has been reported as 2.0 – 5.4 Gy, and recently a value of around 5.0 Gy has been gaining wider acceptance [40, 41]. However, the traditional value of 3.0 Gy is often still used, and this value is indeed safer when dealing with a hypofractionated dose-fractionation model such as HDR, so that $\alpha/\beta = 3.0$ Gy will be used hereafter. In addition, we will use the traditional linear-quadratic (LQ) formula [42]:

$$BED = nd(1 + d/(\alpha/\beta)),$$

where BED = biologically effective dose, n = number of fractions, and d = dose per fraction.

However, we note that for an extremely hypofractionated dose range such as ≥ 6.0 Gy/fraction, compatibility of the LQ formula is not entirely assured. To understand by intuition, we also calculated EQD_{2Gy} as the biologically equivalent dose in 2-Gy fractions.

Until the publication of the previously mentioned paper by Brenner and Hall in 1999, HDR for prostate cancer had

Table 2. Clinical results of prostate HDR brachytherapy as monotherapy

Author [ref.]	Dose fractionation	No. of Patients	Follow-up (year)	PSA control rate/ Risk group	Late toxicity ≥ Grade 2[a]	
					Genitourinary	Gastrointestinal
Yoshioka [submitted for publication, 21]	54 Gy/9 Fr.	112	5.4	85% (5y)/Low 93% (5y)/Intermediate 79% (5y)/High	7.1%	7.1%
	45.5 Gy/7 Fr.	63	3.5	96% (3y)/Intermediate 90% (3y)/High	6.3%	1.6%
Demanes [12]	42 Gy/6 Fr.	157	5.2	97% (5y)/Low–intermediate	28.9%	<1.0%
Martinez [18, 22]	38 Gy/4 Fr.	171	4.6	91% (5y)/Low–intermediate	40.5%	2.0%
	24 Gy/2 Fr.	50	1.4	Not available	25.5%	5.3%
	27 Gy/2 Fr.	44				
Rogers [11]	39 Gy/6 Fr.	284	2.7	94% (5y)/Intermediate	7.7%	0.0%
Zamboglou [10]	38 Gy/4 Fr.	141	4.4	95% (5y)/Low	27.5%	2.6%
	38 Gy/4 Fr.	351		93% (5y)/Intermediate		
	34.5 Gy/3 Fr.	226		93% (5y)/High		
Hoskin [9]	34 Gy/4 Fr.	34	3.5	95% (3y)/Intermediate 87% (3y)/High	33.0%	13.0%
	36 Gy/4 Fr.	25			40.0%	4.0%
	31.5 Gy/3 Fr.	55			34.0%	7.0%
Ghadjar [13]	38 Gy/4 Fr.	36	3	100% (3y)/Low–intermediate	36.1%	5.6%
Barkati [14]	30 Gy/3 Fr.	19	3.3	88% (3y)/Low–intermediate	59.0%	5.1%
	31.5 Gy/3Fr.	19				
	33 Gy/3 Fr.	19				
	34.5 Gy/3 Fr.	22				
Komiya [16]	45.5 Gy/7 Fr.	51	1.4	100% (2y)/Low–high	11.8%	2.0%
Prada [17]	19 Gy/1 Fr.	40	1.6	100% (2.7y)/Low 88% (2.7y)/Intermediate	0.0%	0.0%

HDR = high-dose-rate, PSA = prostate-specific antigen, Fr. = fraction(s). [a]Scored per event not per patient.

been considered disadvantageous in terms of radiation biology because its large fraction size had been associated with more late-tissue damage, as in the case of other cancers, although it was seen as more effective in terms of radiation physics. However, Brenner and Hall's paper resulted in a drastic change due to its astounding assertion that the α/β value of prostate cancer was smaller than that of normal tissue, implying that a hypofractionated dose fractionation regimen such as HDR could be considered advantageous in terms of radiation biology as well. HDR, especially as monotherapy, thus gained recognition as, at least in theory, an excellent method in terms of both radiation biology and physics. As seen in Table 1, only three institutions were using HDR monotherapy in the 1990s [5, 6, 12], whereas eight additional new institutions initiated it in the 2000s [7, 8, 11, 13–17].

Table 1 lists dose fractionations and associated BEDs of monotherapeutic HDR brachytherapy from the literature. The BED for prostate cancer ranges from 208–299 Gy, with a median of 256 Gy. In comparison with LDR brachytherapy, where some practitioners attempted to attain BED > 200 Gy by adding EBRT for a better outcome [43], HDR monotherapy has already achieved BEDs far higher than 200 Gy. The values for EQD_{2Gy} range from 89–128 Gy, with a median of 110 Gy, which may be impossible to administer with EBRT, even when using the most up-to-date IMRT technique. As for late toxicity, EQD_{2Gy} ranges from 72–110 Gy, with a median of 86 Gy, which can be considered the equivalent of the maximum dose of 86.4 Gy administered with the current IMRT [44]. This means that, theoretically, hypofractionation with a large fraction size can enhance BED for prostate cancer without increasing BED for late-responding tissue.

Recent trends are toward a smaller number of fractions and shorter treatment. In the 1990s and the early 2000s, many institutions started using a 4-fraction regimen, for example, 38 Gy/4 fractions [6–8, 13]. However, 3-, 2-, or even 1-fraction regimens have been adopted recently.

Zamboglou *et al.* [10], Hoskin *et al.* [9], and Barkati *et al.* [14] used 30–34.5 Gy/3 fractions (10–11.5 Gy per fraction), and Hoskin *et al.* [9] and Ghilezan *et al.* [18] used 26–27 Gy/2 fractions (13–13.5 Gy per fraction). Prada *et al.* [17] reported their findings for a 19 Gy/1 fraction regimen. Such a single-fraction regimen would maximize the therapeutic ratio, and at the same time would avoid the drawbacks of HDR brachytherapy (hospitalization and needle displacement during the treatment period). However, a single-fraction regimen might, by its very nature, diminish the advantages of fractionation, that is, reoxygenation and redistribution (reassortment). Careful watching thus seems to be essential for such an intriguing new regimen.

Multiple implants constitute an alternative approach. For this procedure, as performed at the California Endocurietherapy [12] and the GammaWest Cancer Services [11], each implant consists of three fractions over two days, after which this set is repeated. A total of 6 fractions are delivered with a moderate fraction size of 6.5–7.0 Gy. At Klinikum Offenbach [10], three implants are used with 11.5 Gy for each implant with a single fraction. At this institution, multi-fraction HDR monotherapy is reportedly completed without hospitalization.

At Osaka University, dose fractionation was changed from 54 Gy/9 fractions to 45.5 Gy/7 fractions in 2005, in conjunction with an increase in fraction size from 6 Gy to 6.5 Gy (Y. Yoshioka *et al.*, submitted for publication). The new schedule involves not only a reduction in the bed confinement period from 5 to 4 days, but also a reduction in BED. The stated reason for reducing the dose was that many clinical results with high biochemical control rates had proven the BED of HDR monotherapy to be high enough, and that the next step should be dose reduction to diminish the toxicity rate without compromising the high control rate.

REPORTED CLINICAL RESULTS

Table 2 lists clinical results of monotherapeutic HDR brachytherapy from the literature. Only 10 institutions worldwide have reported clinical results for prostate HDR monotherapy. The longest median follow-up was 5.4 years, while the median follow-up of most of the studies was only 1–3 years.

The reported 5-year prostate-specific antigen (PSA) control rate for low-risk groups ranged from 85–97%, mostly >90%. For intermediate-risk groups, some authors reported a PSA control rate of 93–94%, and for high-risk groups, it was reported between 79 and 93%, mostly >80%. Although none of these studies have reported a follow-up period much beyond 5 years, the overall PSA control rates reported thus far have been excellent, which may be attributed to the high BED of >200 Gy mentioned above.

The reported toxicity levels were generally acceptable. However, some authors have reported Grade 3 toxicity. Frequency of late genitourinary (GU) toxicity ≥ Grade 2 ranged from 0–59.0%, and for late gastrointestinal (GI) toxicity the rate was 0–13.0%. While late GI toxicity was ≤ 5% in most cases, several authors reported late GU toxicity as high as 20–40%. It should be noted, however, that these values were obtained per event, not per patient; that is, multiple events may have been counted for one patient. Because of the short follow-up period for most of the studies, very little actuarial toxicity data per patient has been available. A comparison with IMRT, for example, would be difficult at present and has to await the availability of more mature clinical data for HDR monotherapy.

HDR AS A PRECEDENT MODEL OF EXTREME HYPOFRACTIONATION FOR STEREOTACTIC RADIOTHERAPY AND PARTICLE THERAPY

A discussion of hypofractionation for prostate cancer would entail a typical fraction size of 2.5–3.0 Gy when a linear accelerator is used. Because HDR monotherapy adopts a much larger fraction size, such as 6–10 Gy or more, some authors refer to it as 'extreme hypofractionation' [21, 45]. Some groups, including Stanford University [46] and a multi-institutional trial in the USA [47], have introduced stereotactic body radiotherapy (SBRT) using e.g. CyberKnife with extreme hypofractionation, with reference to the dose fractionations and clinical results of HDR monotherapy. Some investigators at the CyberKnife Center in San Diego, CA, tested the ability of CyberKnife plans to approximate the dose distribution of HDR brachytherapy and concluded that this was indeed possible, naming the procedure the 'virtual HDR' CyberKnife treatment [48].

Particle therapy, which can be considered a kind of EBRT in terms of extracorporeal administration of ionizing radiation, can yield a better dose distribution as with SBRT. If an excellent dose concentration to the tumor, or a dose that sufficiently spares the adjacent normal tissue can be assured, we would be inclined to proceed to hypofractionation because of patient convenience and medical resource efficiency. Brachytherapy is generally deemed the most appropriate method for testing an unprecedentedly high dose of irradiation, because the dose invariably falls off rapidly due to the inverse square law. In addition, it is not affected by any organ motion either intra- or inter-fractionally. In other words, brachytherapy seems to be the least likely to entail unexpected pitfalls such as the uncertainty of dose distribution caused by the interplay effect when segmented or spotted beams are used in EBRT. It therefore seems reasonable to test an inexperienced BED or dose fractionation with HDR monotherapy first, and then to replace it with SBRT or particle therapy using the findings obtained by

HDR monotherapy, but also moving on to less invasive radiotherapy.

CONCLUSION

HDR monotherapy is a comparatively new brachytherapy method for prostate cancer with a dose distribution that is superior in terms of radiation physics. Furthermore, it can maximize the advantages of hypofractionation in terms of radiation biology. Research on HDR monotherapy is accelerating, with a growing number of publications reporting excellent preliminary clinical results due to the high BED. These findings, obtained by HDR monotherapy as a precedent-setting model of extreme hypofractionation, have recently tended to be used for other radiotherapy techniques, such as SBRT. All of these facts point to the emerging role of HDR brachytherapy as monotherapy for prostate cancer.

FUNDING

This work was supported by the Japan Society for the Promotion of Science (JSPS) KAKENHI (21791192) and the Core-to-Core Program (23003).

REFERENCES

1. Galalae RM, Kovacs G, Schultze J *et al.* Long-term outcome after elective irradiation of the pelvic lymphatics and local dose escalation using high-dose-rate brachytherapy for locally advanced prostate cancer. *Int J Radiat Oncol Biol Phys* 2002;**52**:81–90.
2. Mate TP, Gottesman JE, Hatton J *et al.* High dose-rate afterloading Ir-192 prostate brachytherapy: feasibility report. *Int J Radiat Oncol Biol Phys* 1998;**41**:525–33.
3. Kovács G, Pötter R, Loch T *et al.* GEC/ESTRO-EAU recommendations on temporary brachytherapy using stepping sources for localised prostate cancer. *Radiother Oncol* 2005;**74**:137–48.
4. Yamada Y, Rogers L, Demanes DJ *et al.* American Brachytherapy Society consensus guidelines for high-dose-rate prostate brachytherapy. *Brachytherapy* 2012;**11**:20–32.
5. Yoshioka Y, Nose T, Yoshida K *et al.* High-dose-rate interstitial brachytherapy as a monotherapy for localized prostate cancer: treatment description and preliminary results of a phase I/II clinical trial. *Int J Radiat Oncol Biol Phys* 2000;**48**:675–81.
6. Martinez A, Pataki I, Edmundson G *et al.* Phase II prospective study of the use of conformal high-dose-rate brachytherapy as monotherapy for the treatment of favorable stage prostate cancer: a feasibility report. *Int J Radiat Oncol Biol Phys* 2001;**49**:61–9.
7. Martin T, Baltas D, Kurek R *et al.* 3-D conformal HDR brachytherapy as monotherapy for localized prostate cancer. A pilot study. *Strahlenther Onkol* 2004;**180**:225–32.
8. Corner C, Rojas AM, Bryant L *et al.* A Phase II study of high-dose-rate afterloading brachytherapy as monotherapy for the treatment of localized prostate cancer. *Int J Radiat Oncol Biol Phys* 2008;**72**:441–6.
9. Hoskin P, Rojas A, Lowe G *et al.* High-dose-rate brachytherapy alone for localized prostate cancer in patients at moderate or high risk of biochemical recurrence. *Int J Radiat Oncol Biol Phys* 2012;**82**:1376–84.
10. Zamboglou N, Tselis N, Baltas D *et al.* High-dose-rate interstitial brachytherapy as monotherapy for clinically localized prostate cancer: treatment evolution and mature results. *Int J Radiat Oncol Biol Phys* 2013;**85**:672–8.
11. Rogers CL, Alder SC, Rogers RL *et al.* High dose brachytherapy as monotherapy for intermediate risk prostate cancer. *J Urol* 2012;**187**:109–16.
12. Demanes DJ, Martinez AA, Ghilezan M *et al.* High-dose-rate monotherapy: safe and effective brachytherapy for patients with localized prostate cancer. *Int J Radiat Oncol Biol Phys* 2011;**81**:1286–92.
13. Ghadjar P, Keller T, Rentsch CA *et al.* Toxicity and early treatment outcomes in low- and intermediate-risk prostate cancer managed by high-dose-rate brachytherapy as a monotherapy. *Brachytherapy* 2009;**8**:45–51.
14. Barkati M, Williams SG, Foroudi F *et al.* High-dose-rate brachytherapy as a monotherapy for favorable-risk prostate cancer: a Phase II trial. *Int J Radiat Oncol Biol Phys* 2012;**82**:1889–96.
15. Yoshida K, Yamazaki H, Nose T *et al.* Needle applicator displacement during high-dose-rate interstitial brachytherapy for prostate cancer. *Brachytherapy* 2010;**9**:36–41.
16. Komiya A, Fujiuchi Y, Ito T *et al.* Early quality of life outcomes in patients with prostate cancer managed by high-dose-rate brachytherapy as monotherapy. *Int J Urol* 2013;**20**:185–92.
17. Prada PJ, Jimenez I, González-Suárez H *et al.* High-dose-rate interstitial brachytherapy as monotherapy in one fraction and transperineal hyaluronic acid injection into the perirectal fat for the treatment of favorable stage prostate cancer: treatment description and preliminary results. *Brachytherapy* 2012;**11**:105–10.
18. Ghilezan M, Martinez A, Gustason G *et al.* High-dose-rate brachytherapy as monotherapy delivered in two fractions within one day for favorable/intermediate-risk prostate cancer: preliminary toxicity data. *Int J Radiat Oncol Biol Phys* 2012;**83**:927–32.
19. Yoshioka Y, Nose T, Yoshida K *et al.* High-dose-rate brachytherapy as monotherapy for localized prostate cancer: a retrospective analysis with special focus on tolerance and chronic toxicity. *Int J Radiat Oncol Biol Phys* 2003;**56**: 213–20.
20. Yoshioka Y, Konishi K, Oh RJ *et al.* High-dose-rate brachytherapy without external beam irradiation for locally advanced prostate cancer. *Radiother Oncol* 2006;**80**:62–8.
21. Yoshioka Y, Konishi K, Sumida I *et al.* Monotherapeutic high-dose-rate brachytherapy for prostate cancer: five-year results of an extreme hypofractionation regimen with 54 Gy in nine fractions. *Int J Radiat Oncol Biol Phys* 2011;**80**:469–75.
22. Martinez AA, Demanes J, Vargas C *et al.* High-dose-rate prostate brachytherapy: an excellent accelerated-hypofractionated

treatment for favorable prostate cancer. *Am J Clin Oncol* 2010;**33**:481–8.
23. Roach M, 3rd, DeSilvio M, Lawton C *et al.* Phase III trial comparing whole-pelvic versus prostate-only radiotherapy and neoadjuvant versus adjuvant combined androgen suppression: Radiation Therapy Oncology Group 9413. *J Clin Oncol* 2003;**21**:1904–11.
24. Lawton CA, DeSilvio M, Roach M, III *et al.* An update of the phase III trial comparing whole pelvic to prostate only radiotherapy and neoadjuvant to adjuvant total androgen suppression: updated analysis of RTOG 94-13, with emphasis on unexpected hormone/radiation interactions. *Int J Radiat Oncol Biol Phys* 2007;**69**:646–55.
25. Vargas CE, Galalae R, Demanes J *et al.* Lack of benefit of pelvic radiation in prostate cancer patients with a high risk of positive pelvic lymph nodes treated with high-dose radiation. *Int J Radiat Oncol Biol Phys* 2005;**63**:1474–82.
26. Schulz RJ, Kagan AR. Dose escalation in the radiation therapy of prostate cancer. *Int J Radiat Oncol Biol Phys* 2011;**80**:1289–91.
27. Morikawa LK, Roach M, III. Pelvic nodal radiotherapy in patients with unfavorable intermediate and high-risk prostate cancer: evidence, rationale, and future directions. *Int J Radiat Oncol Biol Phys* 2011;**80**:6–16.
28. Kim MM, Hoffman KE, Levy LB *et al.* Prostate cancer-specific mortality after definitive radiation therapy: who dies of disease? *Eur J Cancer* 2012;**48**:1664–71.
29. Damore SJ, Syed AM, Puthawala AA *et al.* Needle displacement during HDR brachytherapy in the treatment of prostate cancer. *Int J Radiat Oncol Biol Phys* 2000;**46**:1205–11.
30. Hoskin PJ, Bownes PJ, Ostler P *et al.* High dose rate afterloading brachytherapy for prostate cancer: catheter and gland movement between fractions. *Radiother Oncol* 2003;**68**: 285–8.
31. Mullokandov E, Gejerman G. Analysis of serial CT scans to assess template and catheter movement in prostate HDR brachytherapy. *Int J Radiat Oncol Biol Phys* 2004;**58**:1063–71.
32. Simnor T, Li S, Lowe G *et al.* Justification for inter-fraction correction of catheter movement in fractionated high dose-rate brachytherapy treatment of prostate cancer. *Radiother Oncol* 2009;**93**:253–8.
33. Foster W, Cunha JA, Hsu IC *et al.* Dosimetric impact of interfraction catheter movement in high-dose rate prostate brachytherapy. *Int J Radiat Oncol Biol Phys* 2011;**80**:85–90.
34. Kolkman-Deurloo IK, Roos MA, Aluwini S. HDR monotherapy for prostate cancer: a simulation study to determine the effect of catheter displacement on target coverage and normal tissue irradiation. *Radiother Oncol* 2011;**98**:192–7.
35. Brenner DJ, Hall EJ. Fractionation and protraction for radiotherapy of prostate carcinoma. *Int J Radiat Oncol Biol Phys* 1999;**43**:1095–101.
36. Fowler J, Chappell R, Ritter M. Is alpha/beta for prostate tumors really low? *Int J Radiat Oncol Biol Phys* 2001; **50**:1021–31.
37. Brenner DJ, Martinez AA, Edmundson GK *et al.* Direct evidence that prostate tumors show high sensitivity to fractionation (low alpha/beta ratio), similar to late-responding normal tissue. *Int J Radiat Oncol Biol Phys* 2002;**52**:6–13.
38. Wang JZ, Guerrero M, Li XA. How low is the alpha/beta ratio for prostate cancer? *Int J Radiat Oncol Biol Phys* 2003;**55**:194–203.
39. Miralbell R, Roberts SA, Zubizarreta E *et al.* Dose-fractionation sensitivity of prostate cancer deduced from radiotherapy outcomes of 5,969 patients in seven international institutional datasets: α/β=1.4 (0.9–2.2) Gy. *Int J Radiat Oncol Biol Phys* 2012;**82**:e17–24.
40. Brenner DJ. Fractionation and late rectal toxicity. *Int J Radiat Oncol Biol Phys* 2004;**60**:1013–5.
41. Tucker SL, Thames HD, Michalski JM *et al.* Estimation of α/β for late rectal toxicity based on RTOG 94-06. *Int J Radiat Oncol Biol Phys* 2011;**81**:600–5.
42. Fowler JF. The linear-quadratic formula and progress in fractionated radiotherapy. *Br J Radiol* 1989;**62**:679–94.
43. Stone NN, Potters L, Davis BJ *et al.* Customized dose prescription for permanent prostate brachytherapy: insights from a multicenter analysis of dosimetry outcomes. *Int J Radiat Oncol Biol Phys* 2007;**69**:1472–7.
44. Spratt DE, Pei X, Yamada J *et al.* Long-term survival and toxicity in patients treated with high-dose intensity modulated radiation therapy for localized prostate cancer. *Int J Radiat Oncol Biol Phys* 2013;**85**:686–92.
45. Lee WR. Extreme hypofractionation for prostate cancer. *Expert Rev Anticancer Ther* 2009;**9**:61–5.
46. King CR, Brooks JD, Gill H *et al.* Long-term outcomes from a prospective trial of stereotactic body radiotherapy for low-risk prostate cancer. *Int J Radiat Oncol Biol Phys* 2012;**82**:877–82.
47. McBride SM, Wong DS, Dombrowski JJ *et al.* Hypofractionated stereotactic body radiotherapy in low-risk prostate adenocarcinoma: preliminary results of a multi-institutional phase 1 feasibility trial. *Cancer* 2012;**118**: 3681–90.
48. Fuller DB, Naitoh J, Lee C *et al.* Virtual HDR CyberKnife treatment for localized prostatic carcinoma: dosimetry comparison with HDR brachytherapy and preliminary clinical observations. *Int J Radiat Oncol Biol Phys* 2008;**70**:1588–97.

JOURNAL OF APPLIED CLINICAL MEDICAL PHYSICS, VOLUME 14, NUMBER 5, 2013

Gemstone spectral imaging: determination of CT to ED conversion curves for radiotherapy treatment planning

Masashi Yagi,[1a] Takashi Ueguchi,[2] Masahiko Koizumi,[3] Toshiyuki Ogata,[1] Sachiko Yamada,[2] Yutaka Takahashi,[1] Iori Sumida,[4] Yuichi Akino,[1] Koji Konishi,[1] Fumiaki Isohashi,[1] Noriyuki Tomiyama,[5] Yasuo Yoshioka,[1] Kazuhiko Ogawa[1]

Department of Radiation Oncology,[1] Osaka University Graduate School of Medicine, Osaka; Department of Radiology,[2] Osaka University Hospital, Osaka; Division of Medical Physics,[3] Oncology Center, Osaka University Hospital, Osaka; Department of Oral and Maxillofacial Radiology,[4] Osaka University Graduate School of Dentistry, Osaka; Department of Diagnostic and Interventional Radiology,[5] Osaka University Graduate School of Medicine, Osaka, Japan
m.yagi@radonc.med.osaka-u.ac.jp

Received 27 December, 2012; accepted 9 April, 2013

The monochromatic images acquired by Gemstone spectral imaging (GSI) mode on the GE CT750 HD theoretically determines the computed tomography (CT) number more accurately than that of conventional scanner. Using the former, the CT number is calculated from (synthesized) monoenergetic X-ray data. We reasoned that the monochromatic image might be applied to radiotherapy treatment planning (RTP) to calculate dose distribution more accurately. Our goal here was to provide CT to electron density (ED) conversion curves with monochromatic images for RTP. Therefore, we assessed the reproducibility of CT numbers, an important factor on quality assurance, over short and long time periods for different substances at varying energy. CT number difference between measured and theoretical value was investigated. The scanner provided sufficient reproducibility of CT numbers for dose calculation over short and long time periods. The CT numbers of monochromatic images produced by this scanner had reasonable values for dose calculation. The CT to ED conversion curve becomes linear with respect to the relationship between CT numbers and EDs as the energy increases. We conclude that monochromatic imaging from a fast switching system can be applied for the dose calculation, keeping Hounsfield units (HU) stability.

PACS numbers: 87.55.-x, 87.55.ne, 87.57.N-, 87.59.bd

Key words: dual-energy CT, Gemstone spectral imaging, monochromatic image, radiotherapy treatment planning, CT to ED conversion curve

I. INTRODUCTION

The application of computed tomography (CT) in radiotherapy is growing and plays an important role for radiotherapy. In radiotherapy, the information acquired by the CT scanner is mainly used to identify targets and organs at risk (OARs) and determine appropriate dosing.(1)

Recently, dual-energy CT has been commercially available. The dual-energy CT concept was suggested by Hounsfield in 1973.(2) Technological limits such as low rotation speed made it initially difficult to use the scanner clinically. However, subsequent rapid advances in CT technology have resulted in the ubiquitous clinical presence of dual-energy scanners. Dual-energy CT can provide more valuable information such as effective atomic number, electron

[a] Corresponding author: Masashi Yagi, Department of Radiation Oncology, Osaka University Graduate School of Medicine, 2-2 (D10) Yamada-oka, Suita, Osaka, 5650871, Japan; phone: +81-6-6879-3482; fax: +81-6-6879-3489; email: m.yagi@radonc.med.osaka-u.ac.jp